Journal of Engineering Management and Systems Engineering
https://www.acadlore.com/journals/JEMSE

Numerical and Experimental Evaluation of the Mechanical Behavior of FRP-Strengthened Solid and Glulam Timber Beams

Şemsettin Kilinçarslan, Yasemin Şimşek Türker, Mehmet Avcar*

Department of Civil Engineering, University of Süleyman Demirel, 32000 Isparta, Turkey

* Correspondence: Mehmet Avcar (mehmetavcar@sdu.edu.tr)

Received: 07-09-2023 **Revised:** 08-15-2023 **Accepted:** 08-22-2023

Citation: Ş. Kilinçarslan, Y. Ş. Türker, and M. Avcar, "Numerical and experimental evaluation of the mechanical behavior of FRP-strengthened solid and glulam timber beams," *J. Eng. Manag. Syst. Eng.*, vol. 2, no. 3, pp. 158–169, 2023. https://doi.org/10.56578/jemse020303.

Abstract: Wood, notably in the forms of sawn lumber and glued laminated (glulam) timber, serves as a prevalent structural material for lightweight constructions and bridges with short spans. Over time, timber structures might experience deterioration due to factors such as biological attack, ageing, and escalated service loads. In such cases, reinforcing or repairing the compromised timber components can often be more economical than full replacement. Fiber-reinforced polymer (FRP) composites, particularly those strengthened using carbon fiber, present significant potential in enhancing the stiffness or load-carrying capacity of these timber systems. In the present investigation, the bending behavior of both solid and glulam beams, reinforced with carbon FRP composites in a "U" shape at the bottom layer, was studied experimentally and numerically. It was observed that reinforced glulam beams exhibit superior load-carrying capacity, displacement, modulus of rupture, and modulus of elasticity as compared to their unreinforced solid beam counterparts. Even though both types of beams are fabricated from identical materials, the laminated beams demonstrated markedly enhanced bending characteristics. Moreover, the addition of reinforcement to glulam beams showed a substantial improvement in bending performance. Consistency between numerical simulations, conducted using a finite element analysis program, and experimental outcomes was noted. This research suggests that timber materials, when strengthened with fiber-augmented polymer fabrics, can be accurately represented using numerical tools.

Keywords: Composite materials; Reinforcement; Polymer; Timber structures

1 Introduction

Composite materials have played a pivotal role, stretching from early civilizations to the present era. The integration of materials to form composites has historically aimed at harnessing properties superior to their individual components, encompassing enhanced strength, corrosion resistance, flexible designs, durability, and improved strength-to-weight ratios [1–3]. Typically, a composite material consists of one continuous phase interspersed with one or more discontinuous phases [4–7]. The continuous phase is termed the matrix, while the discontinuous phase is labeled as the reinforcement [8–11]. Significant enhancements in mechanical and thermal properties can be achieved when reinforcements, characterized by high modulus and tensile strength, are integrated into a polymer matrix [12, 13].

Composite materials are often categorized based on the matrix used: organic, mineral, or metallic. Examples of organic composites include cardboard (comprising resins and cellulose fibers), laminated tires (a fusion of rubber, steel, organic resins, and fibers such as glass, carbon, and boron), and reinforced plastics (blended with resins and short fibers) [14–16]. Mineral composites are further divided into carbon-carbon composites (combining carbon with carbon fibers), ceramic composites (involving ceramics and ceramic fibers), and concrete (a mixture of cement, sand, and additives) [17]. The last category, metallic composites, typically involves combinations such as aluminum with carbon or boron fibers [18–22].

Such composites have found profound applications across diverse sectors, ranging from packaging and automotive to aviation, biomedicine, and aerospace. Notably, the construction sector has recently identified as a promising avenue for the application of FRP due to attributes like lightweight, corrosion resistance, high strength-to-weight ratios, and exemplary durability [23–25]. FRP, often classified under advanced polymer composites, primarily consists of fibers like glass (GFRP), basalt (BFRP), carbon (CFRP), and aramid, encapsulated within polymer matrix resins like epoxy, polyester, and vinyl esters. Among these, GFRP is predominantly utilized, attributed to its commendable tensile strength relative to steel and cost-effectiveness when juxtaposed with CFRP and BFRP. However, a limitation of GFRP is its elastic modulus, which is observed to be substantially lower than that of structural steel, leading to increased deformations in GFRP-strengthened elements [26, 27].

Historically, wood has been revered as a fundamental construction material [28–32]. Despite the advent of contemporary materials, wood, owing to its lightweight nature, ease of fabrication, and environmental advantages, continues to be prominently utilized. Innovations have led to engineered products like glued-laminated timber, crafted from laminations of graded sawn timber bonded structurally. Glulam offers the advantage of repurposing shorter timber pieces into full-length laminations through structural adhesives. Further, its versatility in terms of shape and size is noteworthy. The structural integrity and strength of glulam beams often surpass those of their individual laminations [33].

However, over time, wood structures are susceptible to deterioration due to factors such as increased service loads, ageing, and biological factors [34–37]. Unlike the corrosion process in steel or concrete, the biological degradation of timber, mediated by enzymatic activity, presents a unique challenge. In such instances, rather than opting for complete replacement, reinforcements or repairs might be more cost-effective [38]. Conventional reinforcement techniques for timber involve steel plates, aluminum plates, or timber patches [39–42], but these can introduce additional dead loads and installation costs. Furthermore, steel elements can undergo corrosion under thermal stresses [43]. In such contexts, FRP composites emerge as a potential solution for timber structures, especially when enhanced stiffness or load-bearing capacities are sought.

An exhaustive review of the literature indicated a focus on the mechanical properties of FRP-reinforced beams, predominantly centered around glued laminated timbers. The current study aims to bridge this gap, offering a comprehensive comparison of solid and bonded laminated timbers. Herein, both experimental and computational approaches are employed to evaluate the bending properties of FRP-reinforced composite beams sourced from spruce tree species. The ensuing sections delineate the material properties, experimental design, and findings, concluding with a summary of insights gained.

Table 1. Mechanical properties of spruce timber and glulam GL24h as per DIN 1052:2008 (values in MPa)

Properties	Spruce	Glulam GL 24h
Bending	11	24
Tension parallel	8.5	16.5
Tension rectangular	0.2	0.5
Pressure parallel	8.5	24
Pressure rectangular	2.5-3	2.7
Shear and torsion	0.9-1.6	2.5
Modulus of elasticity parallel	11000	11,600
Modulus of elasticity rectangular	350	390
Shear modulus	550	720

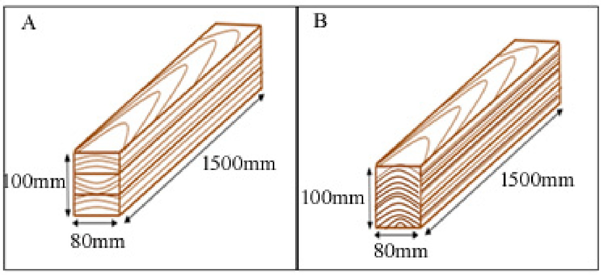

Figure 1. Delineation of beams: (A) The 3-layer glulam beam; (B) The solid glulam beam

2 Methodology

2.1 Materials Properties

For the purposes of this study, 3-layer glulam beams, each measuring 50 mm×80 mm×1500 mm and sourced from Spruce timber, were utilized. These beams were procured from Nasreddin Forest Products (Naswood) located within the Antalya Organized Industrial Zone. Mechanical properties of both the spruce timber and the GL24h glulam, as outlined by DIN 1052:2008, are presented in Table 1. Prior to their utilization in the bending tests, the Spruce beams were conditioned in an environment maintained at 65% relative humidity until an equilibrium humidity of 12% was reached at a consistent temperature of 25°C.

A schematic representation, distinguishing between the solid and glulam beams, is depicted in Figure 1.

The respective serial properties of both solid and composite beams are provided in Table 2.

Table 2. Serial characteristics of the beams under study

Serial-Code	Glulam	Solid	Reinforcement	Moisture Content (%)
S08-10-G-UR	+	-	-	11.62
S08-10-S-UR	-	+	-	11.60
S08-10-G-R	+	-	+	11.71
S08-10-S-R	-	+	+	11.37

To fortify the beams, a carbon FRP composite fabric, labeled as MasterBrace FIB 600/100 CFS, was employed.

2.2 Reinforcement of Solid and Glulam Beams

The reinforcement procedure utilizing FRP fabrics can be delineated in four sequential stages. Initially, the beam surface was meticulously cleaned to ensure the absence of impurities. Following this, a primer was uniformly administered onto the cleansed surface. Approximately 1 to 1.5 hours post the primer application, an adhesive was spread over the primed area. Concluding this preparatory process, fiber polymer fabrics were meticulously wound onto the surface with the freshly applied adhesive. The lower section of the beam received reinforcement in a distinctive U-shape configuration, a schematic of which is portrayed in Figure 2. The carbon-infused MasterBrace FIB 600/100 CFS fabrics, instrumental in the reinforcement, were procured from ÜNAL TEKNİK® Practice Construction Industry and Trade. Ltd. Sti. The technical specifications associated with this fiber-reinforced fabric can be perused in Table 3.

Table 3. Technical specifications of the carbon FRP composite (CFRPC) (MasterBrace FIB 600/100 CFS)

Structure of the Material	Carbon
Modulus of elasticity (MPa)	230000
Tensile Strength (MPa)	4900
Design section thickness (mm)	0.337
Elongation at Break (%)	600
Width (mm)	2,1

For reinforcement, the FRP fabric was methodically applied in three distinct phases, with each phase encompassing three layers of the fabric. A visual representation of the fully reinforced beam is illustrated in Figure 2.

Figure 2. Depiction of the comprehensively reinforced beam

Subsequent to the reinforcement procedure, the beams were left undisturbed for a seven-day duration, after which the bending test was conducted.

2.3 Experimental Flexural Analysis

To ascertain the flexural properties of both solid and composite beams, a 3-point loading method was employed. For precise displacement measurement, an LVDT was strategically positioned at the beam's midpoint. The load cell utilized in the bending tester boasted a capacity of 50 kN, ensuring protection against rupture. Loading was executed at a consistent rate of 6 mm/min. Support points were demarcated at intervals of 300 mm during the tests. Load application and displacement data acquisition were facilitated via a dedicated computer system. A detailed schematic representation of the experimental setup is illustrated in Figure 3, while Figure 4 presents a photograph of the actual setup.

Figure 3. Schematic illustration of the experimental apparatus

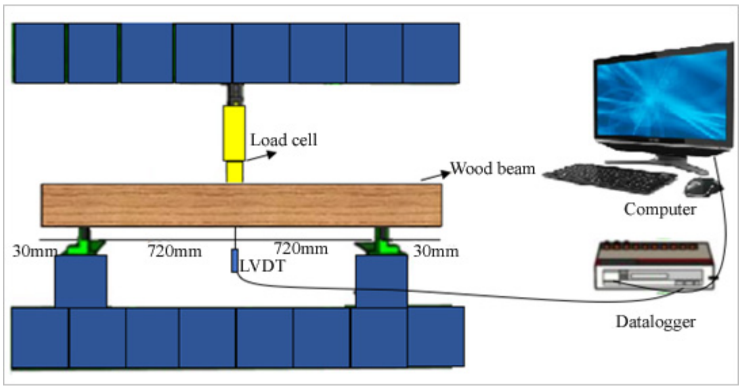

Figure 4. Photographic representation of the experimental apparatus

The flexural strength (σ_e) and the modulus of elasticity (F_{max}) [44] at maximum load break (E) can be represented by:

$$\sigma_e = \frac{3F_{max}L_s}{2bh^2} \tag{1}$$

$$E = \frac{FL_s^3}{4bh^3 f} \tag{2}$$

where, E, F, L, b, h and f denote the modulus of elasticity ($\mathrm{N/mm^2}$), differential of applied forces (N), interval between support points (mm), c (mm) represents the height of the test specimen, and the displacement magnitude (mm), respectively.

Following the experimental procedures, finite element analyses were conducted. Subsequently, comparisons between experimental outcomes and finite element analysis results were drawn.

2.4 Finite Element Analysis

Numerical simulations were executed using the ANSYS 18.1 Standard Solver and the finite element method. Models were developed for both unreinforced and reinforced beams, ensuring that the geometries and loading configurations of these models accurately represented the experimentally tested beams. End conditions were set with pinned and roller supports to confine the vertical movement of the beams. A 25mm rectangular mesh was selected during the modeling phase.

The interface between laminated timbers and FRP was postulated to have a flawless bond. To accurately simulate the simply-supported boundary conditions, restrictions were imposed on select nodes within the beam model.

Utilizing the SOLID45 element, a model was constructed for the timber, an element renowned for 3-D modeling of solid structures1. This element encompasses eight nodes, each equipped with three degrees of freedom across the x, y, and z dimensions. Despite SOLID45's extensive capabilities, encompassing plasticity, stress stiffening, and large deflection among others, capturing the intricate anisotropic behavior of timber remains challenging. Therefore, to approximate the timber's response, orthogonal elastic properties were fed into the software, as portrayed in Figure 5.

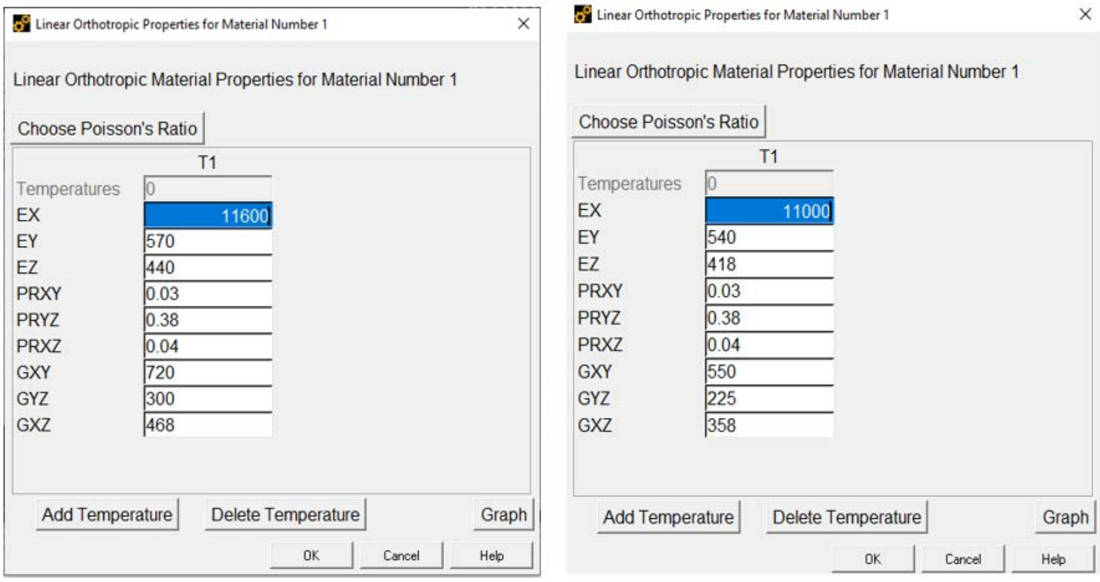

Figure 5. Linear orthotropic material properties: a) Glulam beam; b) Spruce Timber, measured in MPa

The modeling of FRP was undertaken using SOLID65, an eight-node element with three degrees of freedom at each node. Chosen for its capability to forecast tension cracking and compression crushing, SOLID65 is typically employed for modeling reinforced composites including CFRP, concrete, and geological rocks. Given that FRP materials predominantly undergo minute plastic deformation, they were presumed to have linear elastic properties culminating in a brittle failure. The simplified modeling approach highlighted FRP materials as displaying uniaxial linear isotropic behavior. Taking into account the material properties and underlying assumptions, SOLID65 emerged as an apt choice for the accurate representation of their performance. Material properties values were integrated into the software, as depicted in Figure 5.

As the wood laminations in glulam beams were distinctively modeled, it was feasible to incorporate all material attributes. Building upon previous research, which had established impeccable connections between laminations, the ultra-thin melamine formaldehyde adhesive layer was omitted from the model. It was further surmised that the bonds, both between epoxy and FRP and between epoxy and timber, were immaculate, a conclusion derived from the high-quality bonding observed during experimentation. Both wood and FRP were represented as solid finite elements, possessing eight nodes and reduced integration. A mesh of higher granularity was generated around the lamination areas proximate to the FRP reinforcement, which was the principal site for stress transmission from the FRP plate to the glulam. The "tie constraint" was employed to delineate the bond between wood laminations and the wood/epoxy/FRP interfaces. Representative illustrations of these modeled beams can be found in Figure 6.

It should be noted that a linear load, uniformly distributed across the width of the beam, was utilized. Vertical displacement increments were progressively employed for the static small displacement analysis until the pre-specified failure condition was achieved.

3 Results and Discussion

Experimental and numerical investigations were conducted on the bending properties of FRP-reinforced solid and glulam beams derived from spruce tree species. From the numerical analysis, displacement values in relation to single-point loading were observed and are illustrated in Figure 7.

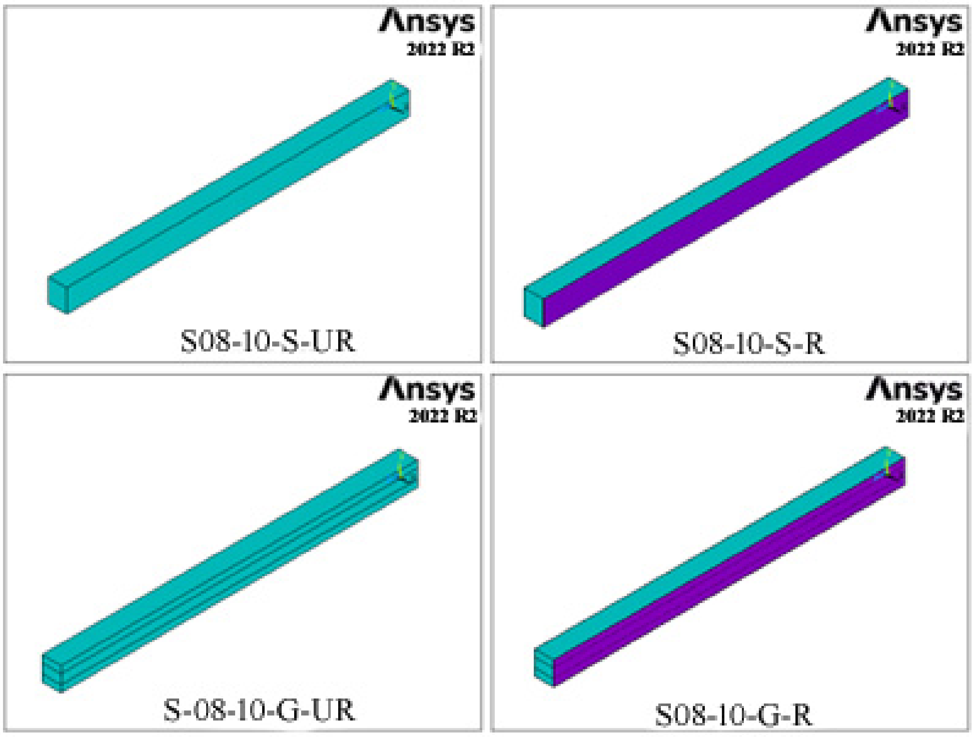

Figure 6. Depictions of the modeled glulam and solid beams

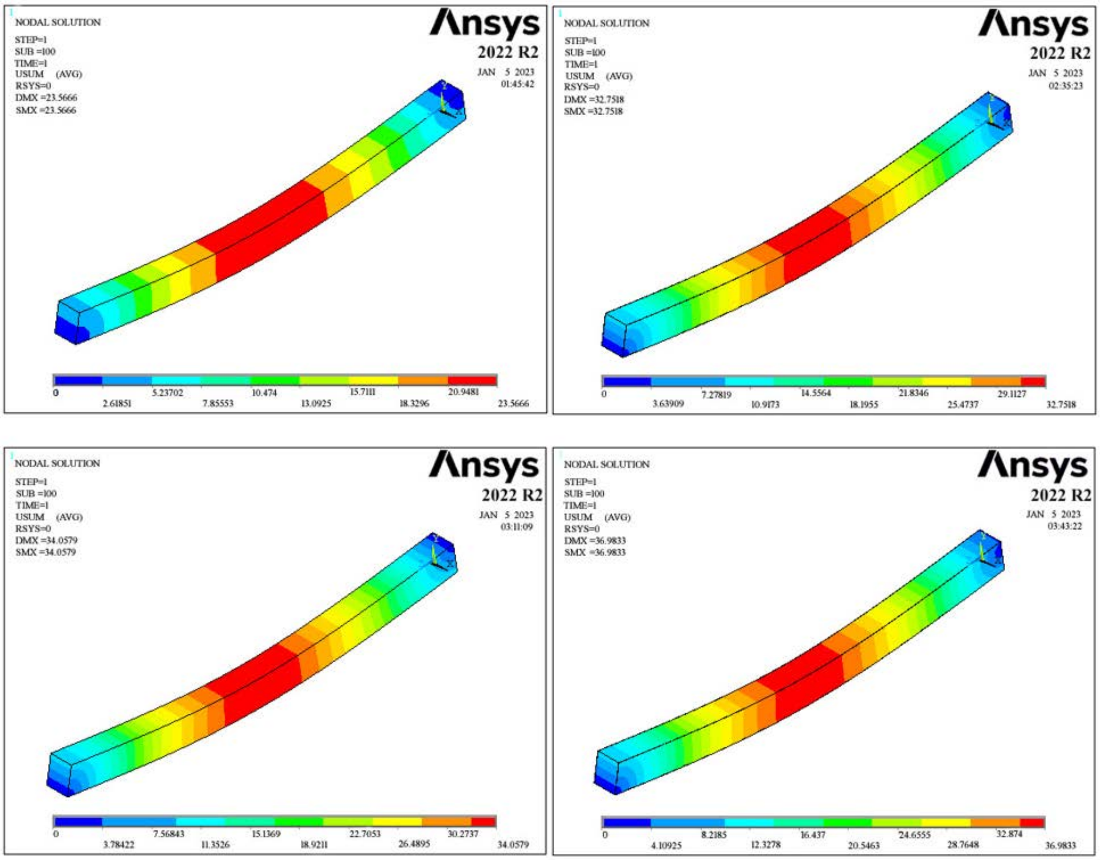

Figure 7. Displacement values derived from ANSYS in relation to single-point loading

Load-displacement curves for S08-10-S-UR (E and A), S08-10-S-R (E and A), S08-10-G-UR (E and A), and S08-10-G-R (E and A) have been provided in Figure 8.

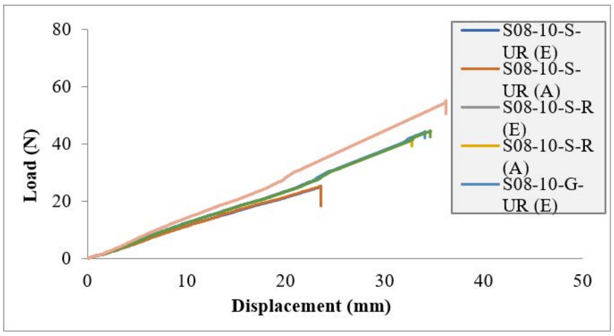

Figure 8. Curves depicting load versus displacement for FRP-reinforced solid and glulam beams

The beam coded as S08-10-G-R exhibited the highest load-carrying capacity, measured experimentally at 54.99 kN, while the beam coded as S08-10-S-UR registered the lowest at 25.14 kN. It was noted that the S08-10-S-R beam demonstrated an increased load-carrying capacity by 65.55% when juxtaposed with the S08-10-S-UR beam. Similarly, a 23.60% increase was discerned in the S08-10-G-R beam in comparison to the S08-10-G-UR beam. An intriguing observation was that the beam coded S08-10-G-UR displayed a surge in load-carrying capacity by 76.96% when contrasted with the S08-10-S-UR beam.

In terms of displacement values, the highest (measured experimentally at 36.18 mm) was attributed to the S08-10-G-R beam. In contrast, the lowest displacement (23.56 mm) was associated with the S08-10-S-UR beam. The S08-10-S-R beam displayed a displacement that was 38.92% greater than its S08-10-S-UR counterpart. A 6% increment in displacement was registered for the S08-10-G-R beam as compared to the S08-10-G-UR beam. An interesting comparison between glulam and solid reference beams revealed that the displacement value for the S08-10-G-UR beam surpassed that of the S08-10-S-UR beam by 30.94%.

Detailed data resulting from the experiments and ANSYS analysis have been tabulated in Table 4, and are visually represented in Figure 9 and Figure 10.

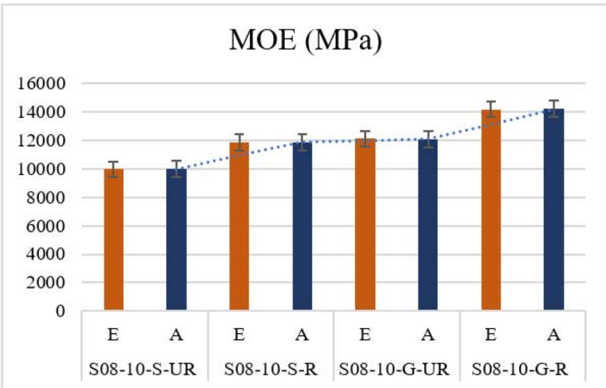

Figure 9. Representation of modulus of elasticity values for FRP-reinforced solid and glulam beams

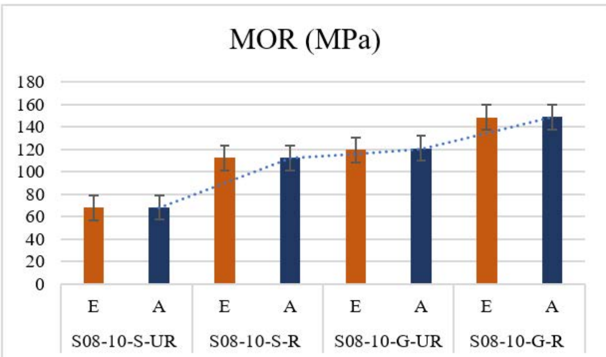

Figure 10. Visualization of modulus of rupture values for FRP-reinforced solid and glulam beams

Table 4. Comprehensive data from experimental outcomes and ANSYS analysis

Experimental				
Sample-Code	**Max Load (kN)**	**Max Deflection (mm)**	**MOE (MPa)**	**MOR (MPa)**
S08-10-S-UR	25.14	23.56	9961	67.87
S08-10-S-R	41.62	32.73	11865	112.37
S08-10-G-UR	44.49	34.12	12117	119.58
S08-10-G-R	54.99	36.18	14182	148.47
ANSYS				
Sample-Code	**Max Load (kN)**	**Max Deflection (mm)**	**MOE (MPa)**	**MOR (MPa)**
S08-10-S-UR	25.24	23.57	9992	68.14
S08-10-S-R	41.64	32.75	11864	112.42
S08-10-G-UR	44.88	34.06	12082	120.96
S08-10-G-R	55.09	36.20	14200	148.74

Within the study parameters, the highest modulus of elasticity, quantified at 14,182 MPa, was attributed to the beam coded as S08-10-G-R. In contrast, the lowest recorded modulus, amounting to 9,961 MPa, was associated with the beam bearing the code S08-10-S-UR. A noteworthy observation was made where the modulus of elasticity for the S08-10-S-R coded beam exhibited an increment of 16% when compared to the S08-10-S-UR counterpart. Similarly, the S08-10-G-R beam displayed a modulus 17.85% greater than the S08-10-G-UR beam. Upon evaluating FRP-reinforced solid and glulam beams, it was discerned that the modulus of elasticity for the S08-10-G-UR coded beam surpassed that of the S08-10-S-UR beam by 17.04%.

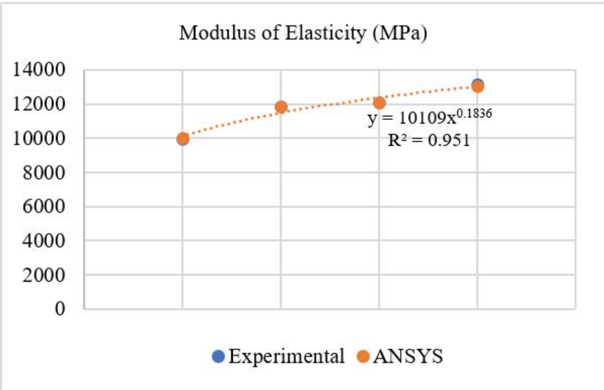

Figure 11. Correlation coefficient (R2) values comparing experimental and ANSYS modulus of elasticity findings

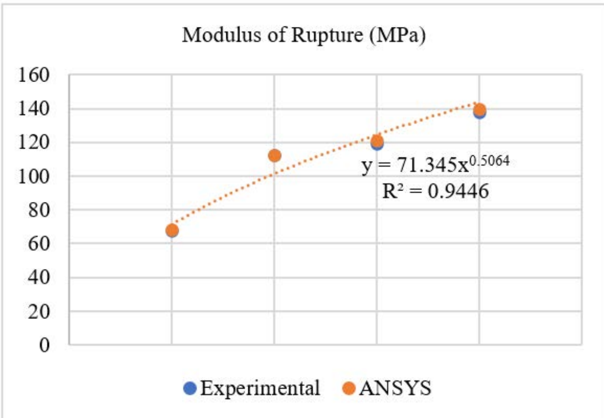

Figure 12. Correlation coefficient (R^2) values comparing experimental and ANSYS modulus of rupture determinations

Regarding the modulus of rupture, the highest recorded value, standing at 148.47 MPa, was associated with the S08-10-G-R beam. The least value, determined at 67.87 MPa, pertained to the beam designated by the code

S08-10-S-UR. The modulus of rupture for the S08-10-S-R coded beam was found to be 39.60% more elevated than its S08-10-S-UR equivalent. The S08-10-G-R coded beam manifested a modulus of rupture 24.15% higher than the S08-10-G-UR coded beam. When the FRP-reinforced solid and glulam beams were juxtaposed, a striking observation was made: the S08-10-G-UR coded beam presented a modulus of rupture 43.24% greater than its S08-10-S-UR counterpart.

Significant coherence was observed between the ANSYS and experimental analysis results, as vividly depicted in Figure 11 and Figure 12.

It was established that the coherence between experimental and ANSYS analyses stood impressively at 0.94 for modulus of rupture values. Furthermore, when scrutinizing the modulus of elasticity values, an almost perfect match at the level of 0.95 was discerned.

4 Conclusion

In the study conducted, bending properties of FRP-reinforced solid and glulam beams derived from spruce tree species were rigorously examined both experimentally and numerically. Superior values in terms of load-carrying capacity, displacement, modulus of rupture, and modulus of elasticity were attributed to the reinforced glulam beams. Conversely, the unreinforced solid beams demonstrated the least values across these parameters.

Upon the reinforcement of solid beams, a surge in the modulus of elasticity by 16% was observed, while the modulus of rupture showcased an increment of 39.60%. Meanwhile, the process of strengthening glulam beams led to a rise in the modulus of elasticity by 17.04% and an ascent in the modulus of rupture by 24.15%. A comparative analysis between solid and glulam beams revealed that the glulam beams' load-bearing capacity exceeded that of solid beams by a staggering 76.96%, and their displacement surpassed by 30.94%. Furthermore, glulam beams presented a modulus of elasticity and a modulus of rupture that were higher by 17.04% and 43.24% respectively, when juxtaposed with their solid counterparts.

From these observations, it was inferred that, despite being fabricated from identical materials, the bending attributes of laminated beams significantly overshadowed those of solid beams. A marked enhancement in bending properties was discernible when glulam beams underwent reinforcement. Both numerical and experimental methodologies yielded congruent outcomes. The augmentation of both glulam and solid materials using fiber fortified with polymer fabrics was determined to be effectively modeled using finite element analysis software.

To bolster the implications of this study, future research could potentially explore how these observed benefits translate into real-world applications, particularly in construction and architectural ventures. Establishing a link between the current findings and existing literature or benchmark studies may also provide a richer context and solidify the research's standing in the academic community.

Funding

This paper was funded by SDÜ BAP (Grant No.: FDK-2019-6950).

Data Availability

The data used to support the findings of this study are available from the corresponding author upon request.

Acknowledgements

This study has been prepared within the scope of the thematic area of "Sustainable Building Materials and Technologies". The authors thank YÖK and YÖK100/2000 program staff.

Conflicts of Interest

The authors declare that they have no conflicts of interest.

References

[1] S. Subhash, M. Uddin, and Prakash, *Introduction, History, and Origin of Composite Materials*. CRC Press, 2022. https://doi.org/10.1201/9781003327370-1

[2] V. P. Van, M. Avcar, M. O. Belarbi, A. Tounsi, and L. Q. Huy, "A new higher-order mixed four-node quadrilateral finite element for static bending analysis of functionally graded plates," *Structures*, vol. 47, pp. 1595–1612, 2023. https://doi.org/10.1016/J.ISTRUC.2022.11.113

[3] Z. Tong-de, Q. Li, B. Yu, C. Huang, Z. Gao, and K. Wang, "Experimental study on dynamic mechanical properties of mortar-sandstone composite under impact load," *Structures*, vol. 51, pp. 1061–1070, 2023. https://doi.org/10.1016/J.ISTRUC.2023.03.086

[4] H. A. P. S. A. Khalil, M. A. Tehrani, Y. Davoudpour, A. H. Bhat, M. Jawaid, and A. Hassan, "Natural fiber reinforced poly (vinyl chloride) composites: A review," *J. Reinforced Plast. Compos.*, vol. 32, no. 5, 2013. https://doi.org/10.1177/0731684412458553

[5] O. Dagdag, R. Hsissou, A. E. Harfi, Z. Safi, A. Berisha, C. Verma, E. E. Ebenso, M. A. Quraishi, N. Wazzan, S. Jodeh, and M. El Gouri, "Epoxy resins and their zinc composites as novel anti-corrosive materials for copper in 3% sodium chloride solution: Experimental and computational studies," *J. Mol. Liquids*, vol. 315, p. 113757, 2020. https://doi.org/10.1016/j.molliq.2020.113757

[6] O. Dagdag, Z. Safi, R. Hsissou, H. Erramli, M. E. Bouchti, N. Wazzan, L. Guo, C. Verma, E. E. Ebenso, and A. E. Harfi, "Epoxy pre-polymers as new and effective materials for corrosion inhibition of carbon steel in acidic medium: Computational and experimental studies," *Sci. Rep.*, vol. 9, no. 1, 2019. https://doi.org/10.1038/s41598-019-48284-0

[7] R. Hsissou, S. Abbout, R. Seghiri, M. Rehioui, A. Berisha, H. Erramli, M. Assouag, and A. Elharfi, "Evaluation of corrosion inhibition performance of phosphorus polymer for carbon steel in [1 m] HCl: Computational studies (DFT, MC and MD simulations)," *J. Mater. Res. Technol.*, vol. 9, no. 3, pp. 2691–2703, 2020. https://doi.org/10.1016/j.jmrt.2020.01.002

[8] A. Mohd, N. Saba, M. Jawaid, M. Nasir, M. Pervaiz, and O. Y. Alothman, "A review on phenolic resin and its composites," *Curr. Anal. Chem.*, vol. 14, no. 3, pp. 185–197, 2018. https://doi.org/10.2174/1573411013666171003154410

[9] H. Rachid, S. Abbout, A. Berisha, M. Berradi, M. Assouag, N. Hajjaji, and A. Elharfi, "Experimental, DFT and molecular dynamics simulation on the inhibition performance of the DGDCBA epoxy polymer against the corrosion of the E24 carbon steel in 1.0 m HCl solution," *J. Mol. Struct.*, vol. 1182, pp. 340–351, 2019. https://doi.org/10.1016/j.molstruc.2018.12.030

[10] W. N. Van de, H. Tekinalp, P. Khanbolouki, S. Ozcan, A. Williams, and M. Tehrani, "Additively manufactured carbon fiber-reinforced composites: State of the art and perspective," *Addit. Manuf.*, vol. 31, p. 100962, 2020. https://doi.org/10.1016/j.addma.2019.100962

[11] H. Rachid, S. Abbout, Z. Safi, F. Benhiba, N. Wazzan, L. Guo, K. Nouneh, S. Briche, H. Erramli, M. Ebn Touhami, M. Assouag, and A. Elharfi, "Synthesis and anticorrosive properties of epoxy polymer for CS in [1 M] HCl solution: Electrochemical, AFM, DFT and MD simulations," *Constr. Build. Mater.*, vol. 270, p. 121454, 2021. https://doi.org/10.1016/j.conbuildmat.2020.121454

[12] S. Amrollahi, B. Ramezanzadeh, H. Yari, M. Ramezanzadeh, and M. Mahdavian, "Synthesis of polyaniline-modified graphene oxide for obtaining a high performance epoxy nanocomposite film with excellent UV blocking/anti-oxidant/anti-corrosion capabilities," *Compos. Part B: Eng.*, vol. 173, p. 106804, 2019. https://doi.org/10.1016/j.compositesb.2019.05.015

[13] K. A. Rod, M. T. Nguyen, M. Elbakhshwan, S. Gills, B. Kutchko, T. Varga, A. M. McKinney, T. J. Roosendaal, M. I. Childers, C. Zhao, Y.-C. K. Chen-Wiegart, J. Thieme, P. K. Koech, W. Um, J. Chun, R. Rousseau, V.-A. Glezakou, and C. A. Fernandez, "Insights into the physical and chemical properties of a cement-polymer composite developed for geothermal wellbore applications," *Cem. Concr. Compos.*, vol. 97, pp. 279–287, 2019. https://doi.org/10.1016/j.cemconcomp.2018.12.022

[14] M. J. Le Guen, R. H. Newman, A. Fernyhough, G. W. Emms, and M. P. Staiger, "The damping–modulus relationship in flax–carbon fibre hybrid composites," *Comp. Part B: Eng.*, vol. 89, pp. 27–33, 2016. https://doi.org/10.1016/j.compositesb.2015.10.046

[15] N. Balakrishnan, M. Arshad, A. Ullah, P. Mertiny, and A. J. Qureshi, "Additive manufacturing ferromagnetic polymers using stereolithography – Materials and process development," *Manuf. Lett.*, vol. 21, pp. 12–16, 2019. https://doi.org/10.1016/j.mfglet.2019.06.003

[16] M. R. Nobile, "15-rheology of polymer–carbon nanotube composites melts," in *Polymer-Carbon Nanotube Composites: Preparation, Properties and Applications*, 2011, pp. 428–481. https://doi.org/10.1533/9780857091390.2.428

[17] M. Asim, M. Jawaid, M. Nasir, and N. Saba, "Effect of fiber loadings and treatment on dynamic mechanical, thermal and flammability properties of pineapple leaf fiber and kenaf phenolic composites," *J. Renew. Mater.*, vol. 6, no. 4, pp. 383–393, 2018. https://doi.org/10.7569/jrm.2017.634162

[18] N. Venkateshwaran and A. Elayaperumal, "Banana fiber reinforced polymer composites - A review," *J. Reinforced Plast. Compos.*, vol. 29, no. 15, pp. 2387–2396, 2010. https://doi.org/10.1177/0731684409360578

[19] H. P. S. Abdul Khalil, M. Jawaid, and A. Abu Bakar, "Woven hybrid composites: Water absorption and thickness swelling behaviours," *BioResources*, vol. 6, no. 2, pp. 1043–1052, 2011.

[20] G. L. Devnani and S. Sinha, "Effect of nanofillers on the properties of natural fiber reinforced polymer composites," *Materials Today: Proceedings*, vol. 18, no. 3, pp. 647–654, 2019. https://doi.org/10.1016/j.matpr.2019.06.460

[21] A. Wael, M. He, Y. Halabi, and K. Y. M. Almajhali, "Optimizing the material and printing parameters of the additively manufactured fiber-reinforced polymer composites using an artificial neural network model and artificial bee colony algorithm," *Structures*, vol. 46, pp. 1781–1795, 2022. https://doi.org/10.1016/j.istruc.202

2.10.134

[22] B. A. Solahuddin and F. M. Yahaya, “A narrative review on strengthening of reinforced concrete beams using carbon fibre reinforced polymer composite material through experimental investigation and numerical modelling,” *Structures*, vol. 52, pp. 666–710, 2023. https://doi.org/10.1016/j.istruc.2023.03.168

[23] L. Yan, X. Yi, T. Yu, and G. Xian, “An overview of structural-functional-integrated composites based on the hierarchical microstructures of plant fibers,” *Adv. Compos. Hybrid Mater.*, vol. 1, pp. 231–246, 2018. https://doi.org/10.1007/s42114-017-0020-3

[24] J. J. Chen and X. U. Gao, “Thermal and electrical anisotropy of polymer matrix composite materials reinforced with graphene nanoplatelets and aluminum-based particles,” *Diamond Relat. Mater.*, vol. 100, p. 107571, 2019. https://doi.org/10.1016/j.diamond.2019.107571

[25] C. Qian, H. Jiang, and Y. Li, “Effect of fiber content and orientation on the scratch behavior of short glass fiber reinforced PBT composites,” *Tribol. Int.*, vol. 146, p. 106221, 2020. https://doi.org/10.1016/j.triboint.2020.106221

[26] A. Farhad, A. Shojaei, S. Dordanihaghighi, E. Jafarpour, S. Mohammadi, and M. Arjmand, “Effects of hybrid carbon-aramid fiber on performance of non-asbestos organic brake friction composites,” *Wear*, vol. 452–453, p. 203280, 2020. https://doi.org/10.1016/j.wear.2020.203280

[27] A. Atefeh, A. Shockravi, H. Rezania, and R. Farahati, “Investigation of anticorrosive properties of novel silane-functionalized polyamide/GO nanocomposite as steel coatings,” *Surf. Interfaces*, vol. 18, p. 100453, 2020. https://doi.org/10.1016/j.surfin.2020.100453

[28] H. T. Sahin, M. B. Arslan, S. Korkut, and C. Sahin, “Colour changes of heat-treated woods of red-bud maple, European hophornbeam and oak,” *Color Res. Appl.*, vol. 36, no. 6, pp. 462–466, 2011. https://doi.org/10.1002/col.20634

[29] C. K. Sahin, M. Topay, and A. A. Var, “A study on suitability of some wood species for landscape applications: Surface color, hardness and roughness changes at outdoor conditions,” *Wood Res.*, vol. 65, no. 3, pp. 395–404, 2020. https://doi.org/10.37763/wr.1336-4561/65.3.395404

[30] C. K. Sahin and B. Onay, “Alternative wood species for playgrounds wood from fruit trees,” *Wood Res.*, vol. 65, no. 1, pp. 149–160, 2020. https://doi.org/10.37763/wr.1336-4561/65.1.149160

[31] J. Lakshmi, E. K. Chakravarthi, P. Sarath Kumar, J. Karingamanna, and K. M. Mini, “Nano filler incorporated epoxy based natural hybrid fiber confinement of concrete systems: Effect of fiber layers and nano filler addition,” *Structures*, vol. 51, pp. 320–331, 2023. https://doi.org/10.1016/j.istruc.2023.03.050

[32] P. Mattipally, A. Maneengam, M. J. Siddique, and R. Selvaraj, “Static and dynamic characteristics of jute/glass fiber reinforced hybrid composites,” *Structures*, vol. 50, pp. 954–962, 2023. https://doi.org/10.1016/j.istruc.2023.01.116

[33] H. Johnsson, T. Blanksvärd, and A. Carolin, “Glulam members strengthened by carbon fibre reinforcement,” *Mater. Struct.*, vol. 40, no. 1, pp. 47–56, 2007. https://doi.org/10.1617/s11527-006-9119-7

[34] D. Pallab and P. Tiwari, “Thermal degradation study of waste polyethylene terephthalate (PET) under inert and oxidative environments,” *Thermochim. Acta*, vol. 679, p. 178340, 2019. https://doi.org/10.1016/j.tca.2019.178340

[35] Z. Dong, T. Zhou, H. Luan, R. C. Williams, P. Wang, and Z. Leng, “Composite modification mechanism of blended bio-asphalt combining styrene-butadiene-styrene with crumb rubber: A sustainable and environmental-friendly solution for wastes,” *J. Cleaner Prod.*, vol. 214, pp. 593–605, 2019. https://doi.org/10.1016/j.jclepro.2019.01.004

[36] B. Y. Min, P. S. Shin, J. H. Kim, H. S. Park, K. L. DeVries, and J. M. Park, “Thermal transfer, interfacial, and mechanical properties of carbon fiber/polycarbonate-CNT composites using infrared thermography,” *Polymer Testing*, vol. 81, p. 106247, 2020. https://doi.org/10.1016/j.polymertesting.2019.106247

[37] D. Soubhik, A. O. Fulmali, P. N. Shivangi, S. Choudhury, R. K. Prusty, and B. C. Ray, “Interface modification of carbon fiber reinforced epoxy composite by hydroxyl/carboxyl functionalized carbon nanotube,” *Materials Today: Proceedings*, vol. 27, pp. 1473–1478, 2020. https://doi.org/10.1016/j.matpr.2020.02.970

[38] V. Datsyuk, S. Trotsenko, G. Trakakis, A. Boden, K. Vyzas-Asimakopoulos, J. Parthenios, C. Galiotis, S. Reich, and K. Papagelis, “Thermal properties enhancement of epoxy resins by incorporating polybenzimidazole nanofibers filled with graphene and carbon nanotubes as reinforcing material,” *Polymer Testing*, vol. 82, p. 106317, 2020.

[39] G. El Mustapha, A. E. Bachiri, S. E. Hegazi, M. Rafik, and A. E. Elharfi, “Thermal degradation of a reactive flame retardant based on cyclotriphosphazene and its blend with dgeba epoxy resin,” *Polym. Degrad. Stab.*, vol. 94, no. 11, pp. 2101–2106, 2009.

[40] R. Hsissou, A. Bekhta, and A. Elharfi, “Viscosimetric and rheological studies of a new trifunctional epoxy pre-polymer with noyan ethylene: Triglycidyl Ether of Ethylene of bisphenol a (TGEEBA),” *J. Mater. Environ.*

Sci., vol. 8, no. 2, pp. 603–610, 2017.

[41] R. Hsissou, A. Bekhta, A. Elharfi, B. Benzidia, and N. Hajjaji, "Theoretical and electrochemical studies of the coating behavior of a new epoxy polymer: Hexaglycidyl ethylene of methylene dianiline (HGEMDA) on E24 steel in 3.5% NaCl," *Portugaliae Electrochim. Acta*, vol. 36, no. 2, pp. 101–117, 2018. https://doi.org/10.4152/pea.201802101

[42] R. Hsissou, A. Bekhta, and A. ElHarfi, "Synthesis and characterization of a new epoxy resin homologous of dgeba: diglycidyl bis disulfide carbon ether of bisphenol A," *J. Chem. Technol. Metall.*, vol. 53, no. 3, pp. 414–421, 2018.

[43] R. Hsissou, A. Elharfi, H. Benassaoui, N. Hajjaji, and F. Benhiba, "Application of a new tri-functional epoxy prepolymer, triglycidyl ethylen ether of bisphenol A in the coating of E24 steel in 3.5% NaCl," *J. Chem. Technol. Metall.*, vol. 52, no. 3, pp. 431–438, 2017.

[44] R. Hsissou, B. Benzidia, N. Hajjaji, and A. Elharfi, "Elaboration and electrochemical studies of the coating behavior of a new nanofunctional epoxy polymer on E24 steel in 3.5% NaCl," *Portugaliae Electrochim. Acta*, vol. 36, no. 4, pp. 259–270, 2018. https://doi.org/10.4152/pea.201804259

Nomenclature

E	modulus of elasticity, $\mathrm{N/mm^2}$
F	difference of applied forces, N
L_s	spacing between support points, mm
b	the width of the test sample, mm
h	height of the test specimen, mm
f	displacement amount, mm
σ_e	flexural strength, $\mathrm{N/mm^2}$
$\mathrm{F_{max}}$	for maximum load at break